A Hybrid Renewable Energy System Management Using an Artificial Intelligence MIMO-Fuzzy Controller

Ilham Aouaci
Smart Grids and Renewable Energies Laboratory, Tahri Mohammed University of Bechar, BP 417, 08000 Bechar, Algeria
aouaci.ilham@univ-bechar.dz (corresponding author)

Boumediene Allaoua
Smart Grids and Renewable Energies Laboratory, Tahri Mohammed University of Bechar, BP 417, 08000 Bechar, Algeria
allaoua.boumediene@univ-bechar.dz

Bousmaha Bouchiba
Smart Grids and Renewable Energies Laboratory, Tahri Mohammed University of Bechar, BP 417, 08000 Bechar, Algeria
bouchiba.bousmaha@univ-bechar.dz

Received: 15 March 2025 | Revised: 22 April 2025 and 9 June 2025 | Accepted: 21 June 2025

 DOI: https://doi.org/10.48084/etasr.10952

ABSTRACT

The integration of clean energy sources into standalone power systems requires the selection of appropriate renewable resources based on the local weather conditions, geographic location, and installation costs. Photovoltaic (PV) panels and hydrogen-based systems, particularly those using Solid Oxide Fuel Cells (SOFCs), are often used in a complementary manner. The efficient operation of such hybrid systems necessitates an intelligent energy management capable of optimizing the power flow to the electrical loads and of storing the surplus energy. To achieve a high power quality and reduce the overall system costs, a suitable system architecture and advanced control strategies are essential. In this context, an intelligent supervisory control based on Multi-Input Multi-Output Fuzzy Logic Control (MIMO-FLC) is proposed. This controller addresses key challenges, such as enhancing the energy efficiency, ensuring a smooth production-consumption balance, and maintaining the service continuity and reliability. The proposed MIMO-FLC effectively manages the hybrid energy system by adapting to the changing weather conditions and load demands. The system was modeled and simulated using MATLAB/Simulink. The simulation results demonstrate that the fuzzy logic-based control significantly improves the system performance, ensuring high power quality and efficient energy usage. The controller successfully directs energy either to the load or to the battery storage without power loss or interruptions. This study emphasizes the simulation process and analyzes the evolution of key parameters—such as power, voltage, pressure, and current density—over time to estimate the electrical energy required for a 1 MW output load.

Keywords-hybrid energy system management; Solid Oxide Fuel Cell (SOFC); PV; energy storage; grid on/off; MIMO-FLC

I. INTRODUCTION

In the pursuit of climate stabilization and global warming reduction, renewable energy will play a vital role. Advancements in technology are expected to lower the costs of clean energy generation while reducing the noise emissions and maintenance requirements. In line with this vision, the Algerian government has initiated sustainable investments by installing large-scale PV farms and hydrogen power plants in the southern regions of the country. The primary goal is to empower isolated villages to produce their own electricity without relying on an interconnected national grid [1, 2].

A hybrid energy system combining solar PV panels and hydrogen-based SOFC is particularly promising. However, both energy sources are inherently intermittent and fluctuate with the weather conditions. Therefore, integrating PV and

hydrogen systems is essential to ensure a continuous and stable power supply, regardless of the load variation or environmental changes [1-3].

To balance generation and consumption and to meet the growing energy demands, utility companies are adopting standalone renewable energy systems. These systems often face challenges, such as frequency instability and voltage sags, caused by mismatches between the power generation and load demand, which complicates their management [4, 5]. Additionally, the use of power electronic devices introduces harmonics into the system, requiring advanced management strategies to maintain the power quality.

To address these challenges, various multi-source system architectures have been developed, incorporating intelligent control techniques, such as Fuzzy Logic Control (FLC). These methods are well-suited to standalone applications and offer robust performance [6]. Mathematical modeling enables the simulation and control of different energy sources. For nonlinear systems, FLC is particularly effective in regulating the PV output, frequency stability, battery current, and overall system voltage [7, 8].

Moreover, the Maximum Power Point Tracking (MPPT) methods are critical for optimizing efficiency. However, traditional MPPT techniques face limitations due to the unpredictable nature of the climatic variables and the degradation of PV panels over time, which affects proportional constants. As a result, intelligent MPPT algorithms are used to improve performance, even under variable environmental conditions.

In this work, the proposed hybrid system—comprising PV, SOFC, and battery storage—was modeled and simulated using MATLAB/Simulink, specifically designed for isolated sites. This integrated approach provides a viable solution for generating clean, reliable energy while contributing to the reduction of the greenhouse gas emissions [9]. Such hybrid systems offer the potential for decentralized and sustainable power generation, making them suitable for various applications, from residential and commercial buildings to microgrids and off-grid communities. They not only contribute to reducing the carbon emissions, but also enhance energy security, increase resilience, and foster energy independence. However, both SOFCs and solar panels have intermittent power generation characteristics as they rely on external factors, such as fuel availability or sunlight. At this point, the storage battery plays a crucial role by functioning as an energy reservoir, capturing and storing excess electricity during periods of high generation and releasing it during times of high demand or when the solar and fuel cell output is low.

Against this background, the present study aims to numerically investigate, using MATLAB-Simulink, a comprehensive hybrid energy system composed of the following components:

- SOFC
- PV system
- Storage system consisted of a Nickel-Metal Hydride (NiMH) battery

The study contains a hybrid system with a SOFC/PV/battery storage managed by an intelligent power manager based on FLC. There are two important aspects of this study, first, the global system architecture is defined for the development of a multi-source system that integrates various renewable energy sources. Second, an intelligent power management strategy is detailed using a MIMI-FLC controller. Based on the weather conditions, this system determines multiple operating modes, allowing the power contribution of each energy source to be identified.

II. HYBRID ENERGY SYSTEM ARCHITECTURE

The architecture system is configured by a DC bus. The power management control of the hybrid system uses FLC to satisfy the load and ensure the continuity and the power supply efficiency, this strategy maintains the state of the charge battery bank, in this way the life time of the battery is extended. Figure 1 presents the global architecture of the hybrid energy system. The hybrid system and storage system are created to assure the power supply of a stand-alone site. The resources chosen have a complementary characteristic; the production of hydrogen energy is stable during the daylight hours, while the production of PV energy follows the fluctuations during the day in the form of climate changes, such as clouds blocking the sun, and stops at night due to the lack of radiation [10].

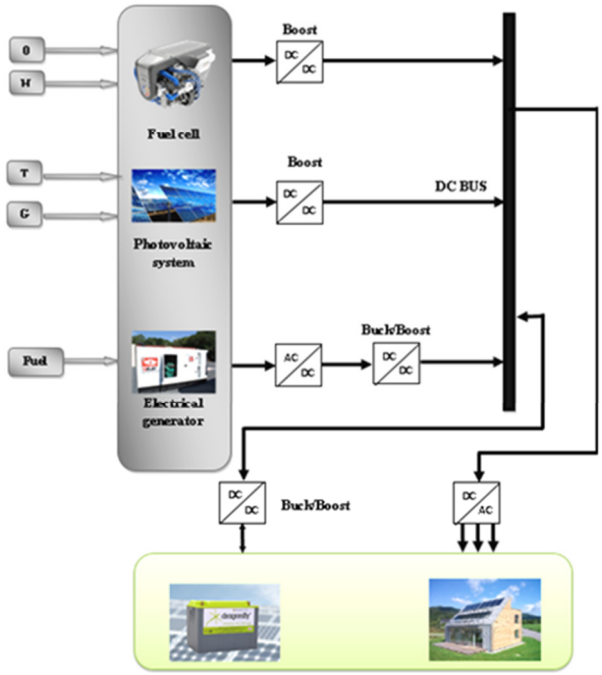

Fig. 1. Architecture of the proposed energy system: O: Exogenous inputs, H: Hydrogen inputs, T: Absolute temperature, G: PV generator, DC: Direct Current; AC: Alternative Current.

The hybrid energy system and storage system are created to assure a load power with 1 MW. The system consists of a SOFC, a PV system, and a storage battery. It includes three

main power elements: a 1 MW load, hybrid power generation from the SOFC and PV system, and an NiMH battery serving as the energy storage unit

Each one of them is pair-connected to a boost converter, which raises the current capacity to a higher level while maintaining a continuous current. However, before reaching the load, the system includes a transducer that converts the current from DC to AC. The SOFC and PV system complement each other, as the PV system does not work at night. SOFCs, therefore, replace them and by adding their voltages together, the required voltage at the load power is reached. An NiMH battery is used to store the excess electrical energy generated by the system. This load power is described by:

$$P_L = P_{SOFC} + P_{PV} \pm P_{Batt} \quad (1)$$

where P_L is the load power (load demand), P_{SOFC} is the SOFC power, P_{PV}: is the PV system power, and P_{Batt} is the storge battery power.

There are two operating modes: $P_{Batt} > 0$ when the battery is charged, and $P_{Batt} < 0$ when the battery is discharged.

III. MODELING OF THE HYBRID ENERGY SYSTEM PARTS

The hydrogen OSFC and PV hybrid system are made up of many components that interact with each other in various ways using power electronic converters, but within the constraints set by the numerous strategies employed to govern the system as a whole and manage it to ensure an adequate power flow for the consumer. This section presents a master model of the SOFC and PV panel, as well as to investigate the properties and mechanism of action of these models.

A. Modeling of Solid Oxide Fuel Cell

A dynamic model of a SOFC stack based on the water flow (PH2O), hydrogen flow (PH2), and oxygen flow (PO2) is shown by [3, 11]:

$$\frac{dP_{H_2O}}{dt} = -\frac{1}{\tau_{H_2O}} P_{H_2O} + \frac{1}{\tau_{H_2O} K_{H_2O}} \left(q_{H_2O}^{in} - 2K_r l_i\right) \quad (2)$$

$$\frac{dP_{H_2}}{dt} = -\frac{1}{\tau_{H_2}} P_{H_2} + \frac{1}{\tau_{H_2} K_{H_2}} \left(q_{H_2}^{in} - 2K_r l_i\right) \quad (3)$$

$$\frac{dP_{O_2}}{dt} = -\frac{1}{\tau_{O_2}} P_{O_2} + \frac{1}{\tau_{O_2} K_{O_2}} \left(q_{O_2}^{in} - 2K_r l_i\right) \quad (4)$$

$$N_0 \left(E_0 + \frac{RT}{2F}\left[ln \frac{P_{H_2} P_{O_2}^{0.5}}{P_{H_2O}}\right]\right) \quad (5)$$

Figure 2 depicts current and voltage relation given by the SOFC stack dynamic model.

B. Modeling of Photovoltaic

The operation of the PV module is represented using the Shockley's "standard" one-diode model, which is generalized to a single PV cell by considering it as a set of identical cells connected in series or parallel [10, 12]. The cell's current is given by:

$$I = I_{ph} + \frac{V - R_S I}{R_{sh}} + I_S \left[exp\left(\frac{q(V - R_S I)}{AKT} - 1\right)\right] \quad (6)$$

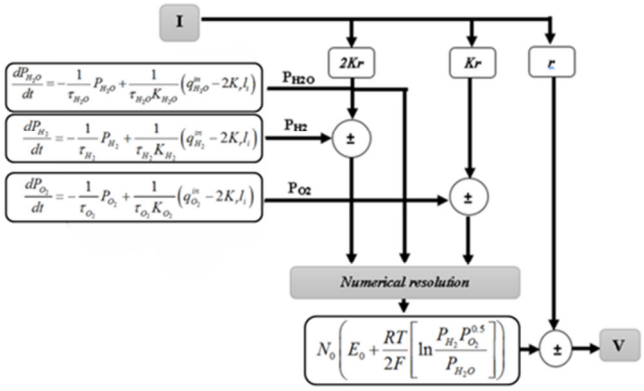

Fig. 2. Current and voltage relation on SOFC stack dynamic model.

These two resistances are related to the electrode elaboration technology. *RS* should be minimized so that R_{Sh} is very large, the photo current I_{ph} changes with irradiance and is computed in proportion to the values supplied at reference conditions:

$$I_{ph} = \frac{\Phi}{\Phi_{ref}} \left[I_{ph_{ref}} + \mu_{Isc}\left(T - T_{ref}\right)\right] \quad (7)$$

where μ_{Isc} is the temperature coefficient of the photocurrent (or short circuit current), which is frequently provided by the manufacturer. It is normally positive but very low. The diode's saturation current is assumed to vary with temperature using [12, 13]:

$$I_S = I_{S_{ref}} \left(\frac{T}{T_{ref}}\right)^3 exp\left[\frac{qE_g}{AK}\left(\frac{1}{T_{ref}} - \frac{1}{T}\right)\right] \quad (8)$$

Φ and Φ_{ref} are the external conditions for which the basic data used to create the model (voltage V_{max}, current I_{max}) maximum are defined. These are either the manufacturer's specifications, which are always given at standard test conditions [12-15].

C. Modeling of Storage Battery

The NiMH model contains two phases, the charging phase and the discharging phase [16]. The discharge model created when $i^* > 0$ is given by:

$$E_{Charge} = E_0 - K \cdot \frac{Q}{Q - it} \cdot i^* - K \cdot \frac{Q}{Q - it} \cdot it + Laplace^{-1}\left(\frac{Exp(s)}{Sel(s)} \cdot 0\right) \quad (9)$$

and the charge model created when ($i^* < 0$) is given by:

$$E_{Discharge} = E_0 - K \cdot \frac{Q}{|it| - 0.1 \cdot Q} \cdot i^* - K \cdot \frac{Q}{Q - it} \cdot it + Laplace^{-1}\left(\frac{Exp(s)}{Sel(s)} \cdot \frac{1}{s}\right) \quad (10)$$

In the battery model, E_{Batt} represents the nonlinear voltage (V), E_0 is the constant voltage component, $E_{xp(s)}$ denotes the exponential zone dynamics (V), $S_{el(s)}$ indicates the battery operating mode: ($S_{el(s)} = 0$ during battery discharge, $S_{el(s)} = 1$ during battery charging), K refers to the polarization constant (Ah-1) or polarization resistance (Ohms), i^* represents the low-frequency current dynamics (A), i is the battery current (A), it is the extracted capacity (Ah), Q is the maximum battery capacity

(*Ah*), *A* is the exponential voltage (*V*), and *B* is the exponential capacity (*Ah-1*) [16].

The parameters of the equivalent circuit, as illustrated in Figure 3, can be adjusted to model different battery types, depending on their discharge characteristics. A typical battery discharge curve consists of three distinct regions, as shown in Figure 3.

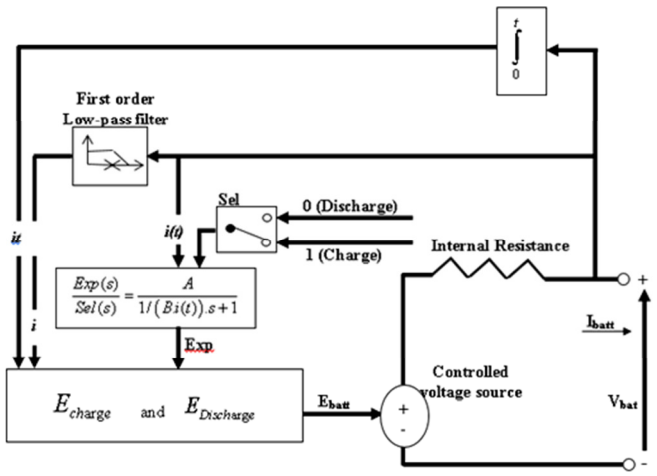

Fig. 3. Equivalent circuit of NiMH battery.

D. DC-DC Converter Modeling

The modeling of this converter includes the analysis of the various operation sequences that will be assumed to have a fixed switching period. Two operating sequences are distinguished according to the status of the Insulated-Gate Bipolar Transistor (IGBT), denoted as *S*. Differential equations can represent these states as [17]:

When S is closed:

$$\begin{cases} L\frac{di_{fc}}{dt} = v_{fc} \\ C_{eq}\frac{dv_{dc}}{dt} = -i_{d2}^{'} - i_{d2} \end{cases} \quad (11)$$

When S is open:

$$\begin{cases} L\frac{di_{fc}}{dt} = v_{fc} - v_{dc} \\ C_{eq}\frac{dv_{dc}}{dt} = i_{fc} - i_{d2}^{'} - i_{d2} \end{cases} \quad (12)$$

The systems of (11) and (12) can be represented by a single system of equations by assuming $u = 0$ when the transistor is open, and $u = 1$ when the transistor is closed, as demonstrated in:

$$\begin{cases} L\frac{di_{fc}}{dt} = v_{fc} - (1-u)v_{dc} \\ C_{eq}\frac{dv_{dc}}{dt} = i_{fc}(1-u) - i_{d2}^{'} - i_{d2} \end{cases} \quad (13)$$

The instantaneous model of the boost converter exhibits nonlinear behavior due to the interaction between the control signal u and the state variables v_{dc} and i_{fc}. This nonlinearity arises from the multiplicative terms involving these variables. To simplify the analysis and facilitate the control design, an average model of the converter is derived by replacing the instantaneous control signal u with its average value over one switching period:

$$T_c = \frac{1}{f_c} \quad (14)$$

$$\begin{cases} L\frac{di_{fc}}{dt} = v_{fc} - (1-D)v_{dc} \\ C_{eq}\frac{dv_{dc}}{dt} = i_{fc}(1-D) - i_{d2}^{'} - i_{d2} \end{cases} \quad (15)$$

with *D* being the duty cycle [17].

The DC-DC converter converts the power from the SOFC/PV to a regulated and controlled DC output at the desired voltage magnitude. In Figure 4, which displays the boost converter power circuit, the DC input voltage is connected in series with an inductor *L*, which works as a current source. In parallel with the current source, a switch *S* turns ON and OFF periodically, supplying energy from the inductor and the source to increase the average output voltage [17].

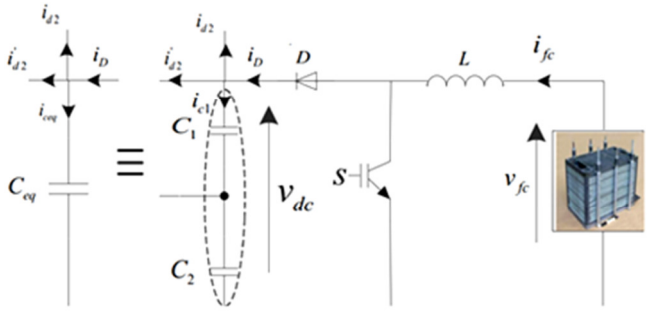

Fig. 4. DC-DC Boost converter.

IV. MANAGEMENT STRATEGY USING MIMO-FLC

The objective of the energy management strategy is to continuously meet the load demand under varying weather conditions while ensuring that the system operates under optimal conditions. The control strategy is designed to manage the power flow by either supplying energy to the load or storing the excess energy in the battery [18, 19].

Table I presents the fuzzy controller rule base, where the linguistic variables used are: Negative Large (NL), Negative Medium (NM), Negative Small (NS), Zero (Z), Positive Small (PS), Positive Medium (PM), and Positive Large (PL). The static DC-DC converter is used to regulate the battery voltage and to limit the current to a maximum value defined during the charge-discharge cycles [20, 21]. During the load phase, the difference between the actual battery voltage and the reference voltage is used to generate the battery's reference current.

The energy stored in the battery is calculated using:

- $P_{Batt} > 0$: When the battery is charged,
- $P_{Batt} < 0$: When the battery is discharged.

TABLE I. RULE BASE FOR THE FUZZY LOGIC CONTROLLER

E/De	NL	NM	NS	Z	PS	PM	PL
NL	PL	PL	PL	PL	Z	Z	Z
NM	PL	PL	PL	PM	PS	Z	Z
NS	PL	PM	PS	PS	PS	Z	Z
Z	PL	PM	PS	Z	NS	NM	NL
PS	Z	Z	NM	NS	NS	NM	NL
PM	Z	Z	NS	NM	NL	NL	NL
PL	Z	Z	NM	NL	NL	NL	NL

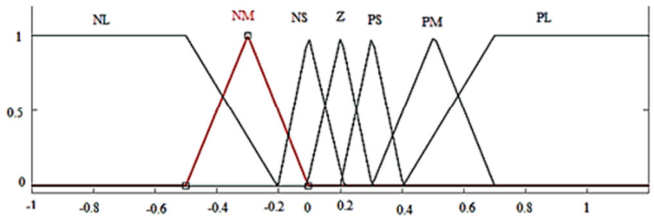

Fig. 5. Membership Functions of E, DE, and DU.

The controller contains two inputs (E and DE) and six outputs. The current membership functions are defined in Figure 5. The relationship between the inputs and outputs can be understood using the surface waveform. Figure 6 shows the surface waveform of the proposed MIMO-FLC.

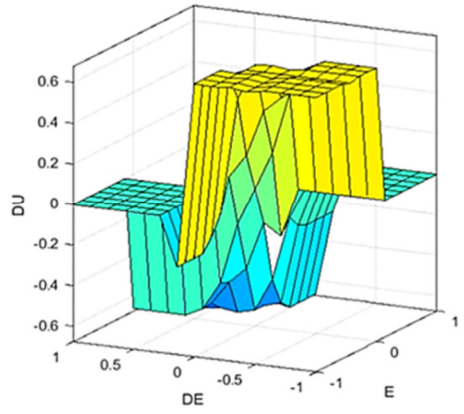

Fig. 6. Surface waveforms of proposed MIMO-FLC.

V. SIMULATION RESULT AND DISCUSSION

Simulation and mathematical modeling are essential tools for developing various power generation devices, and they become even more critical in the context of hybrid systems. This increased importance emerges from the inherent complexity of components, such as SOFC and PV cells. The complexity arises because electrochemical reactions in both SOFC and PV modules are tightly coupled, while the electrical conduction, ionic conduction, and heat transfer processes occur simultaneously within the SOFC. Therefore, a comprehensive analysis of such hybrid systems demands a multidisciplinary approach.

Simulating these hybrid systems improves the accuracy of the result interpolation and extrapolation, providing valuable insights for the system design and optimization. Numerous simulation studies have been performed using different software tools to model these systems effectively.

This study focuses on simulating the hybrid energy system using MATLAB/Simulink. The primary goal of the simulation is to estimate the electrical energy required to generate an output voltage corresponding to a 1 MW load, while tracking the temporal evolution of the power, voltage, pressures, and current density. Using the component models previously described, a test-bed simulation of the proposed hybrid energy system was developed in MATLAB/Simulink. The simulation results demonstrate the system's performance.

A. Power Consumption

Figure 7 portrays the irradiation power during the charge and the discharge scenarios. In both scenarios, the irradiation power will increase and then decreases (the start-up of the system) until it is fixed at 967.9 W, which is the approximate value of the 1000 W given in this study.

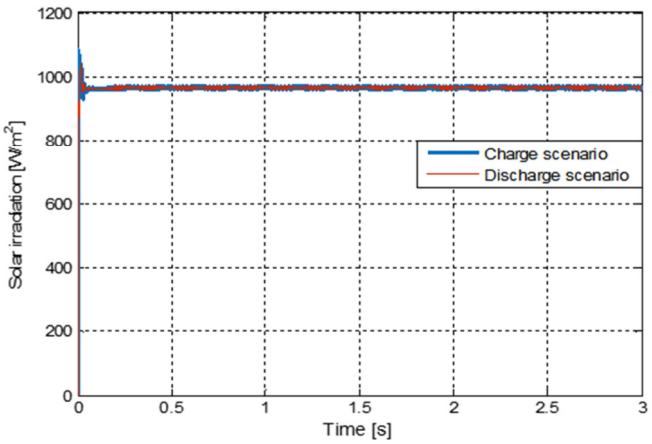

Fig. 7. Solar irradiations.

Figure 8 presents the evolution of the hybrid system powers in the charge scenario as a function of time. At first, the AC system demands a considerable power where it produces 1.533×10^6 W, 1.082×10^6 W, 4.577×10^4 W, 1.039×10^4 W. Then decreases again and is stabilized at 9.998×10^5 W, 9.643×10^5 W, 6.731×10^4 W, -2.009×10^4 W. These results validate (1), as $P_L = P_{SOFC} + P_{PV} - P_{Batt} = 9.643\times10^5 + 6.731\times10^4 - 2.009\times10^4 = 1.001\times10^6 \approx 9.998\times10^5$ W. Figure 9 illustrates the evolution of the hybrid system powers in the discharge scenario.

The load power maintains the same values, while the value of the SOFC decreases to 6.774×10^5 W. The PV decreases from 954.1×10^5 W to -1.431×10^5 W and then increases to 2.963×10^5 W at 0.2144 s. The value of the battery rises to 3.322×10^4 W. It is observed that this value is positive, indicating that the system is operating in a discharge scenario. These results also validate (1), as $\rightarrow 6.774\times10^5 + 2.963\times10^5 - +3.322\times10^4 = 1.007\times10^6 \approx 9.998\times10^5$ W.

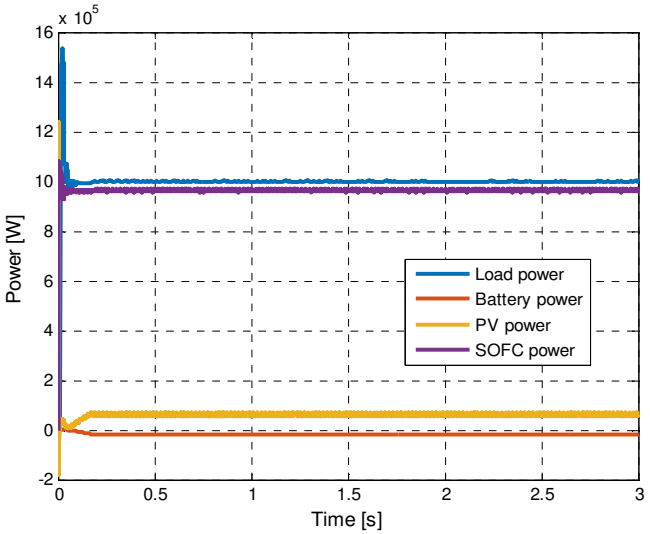

Fig. 8. Evolution of the hybrid system powers in the charge scenario.

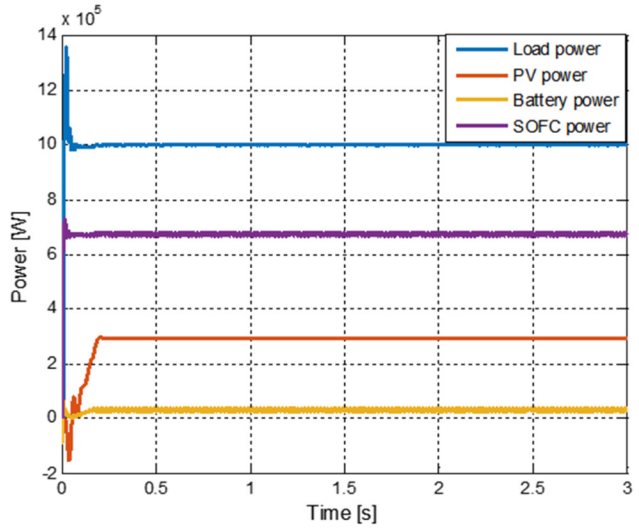

Fig. 9. Evolution of the hybrid system powers in the discharge scenario.

B. Balanced Voltages for Charge and Discharge

Figures 10 (a) and 10 (b) show the Nernst voltage for the charge and the discharge scenario, respectively.

In both the charging and discharging, Nernst voltage increases from 2.228 V, 1.114 V to 2.257 V, 1.125V. Then it decreases again to 2.22 V at 0.228 s, 1.111 V at 0.152 s, and after that it increases again to 2.234 V, 1.118 V. This proves the validity of the proposed system, as the Nernst voltage values do not exceed 2.83 V. The voltage values during discharging are lower, because the battery works to assist the fuel cell.

Figures 11 (a) and 11 (b) present the different voltages in the charging and the discharging scenarios, respectively. In the charging scenario, the load power, SOFC (input and output), and PV increase from 0.075 V, -84.54 V, -72.15 V, 109.8 V to 725.7 V, 330.8 V, 725.7 V, 528.5 V (the start-up of the system). Then it starts decreasing and stabilizes at 651.8 V at 0.188 s, 344.8 V at 0.237 s, 651.8 V at 0.188 s, and 428.1 V at 0.229 s, as a steady state of the system. In the discharging scenario, the same behavior is noted.

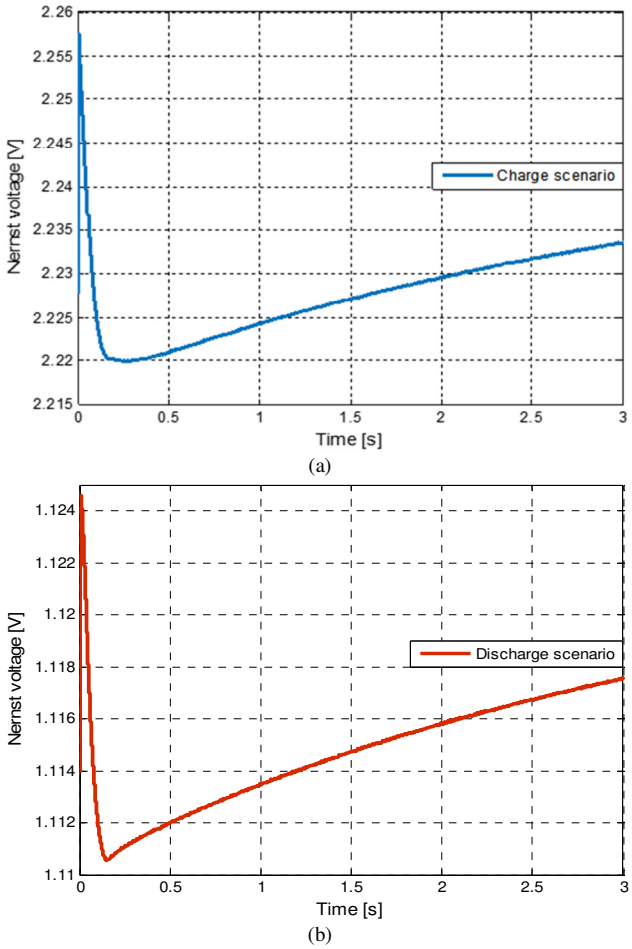

Fig. 10. Nernst Voltage: (a) in the charge scenario, (b) in the discharge scenario.

Figures 12 and 13 illustrate the supply voltage of the bus for the charging and the discharging scenarios respectively, where the supply voltage consists of the three levels that our load power needs. It has a lower value in less time, which results in better sinusoidal.

C. Balanced Currents for Charge and Discharge Time

Figure 15 shows SOFC currents in the charge and the discharge scenario. In charge simulation scenario, the SOFC current decreases from 5091 A to -227.9 A for the start-up of the system, and then increases to a value of 165.3 A at 0.1844 s at which it is stabilized. The SOFC current in discharge simulation scenario takes the same path, but with greater values.

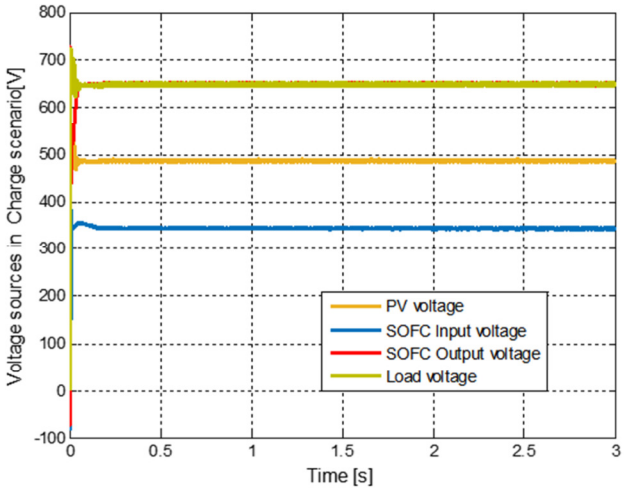

(a)

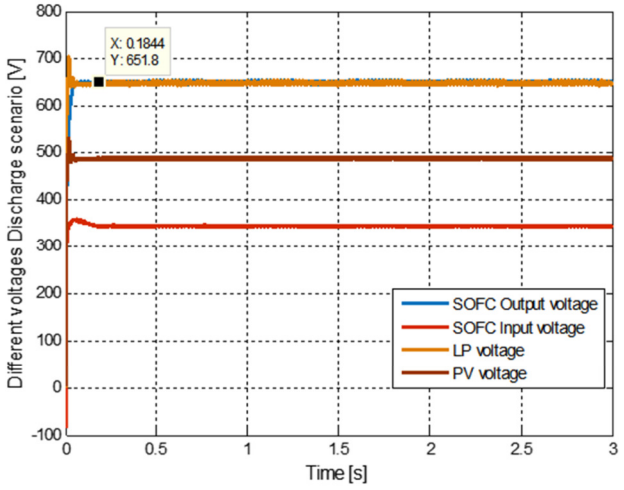

(b)

Fig. 11. (a) Voltages in the charging scenario, (b) voltages in the discharging scenario.

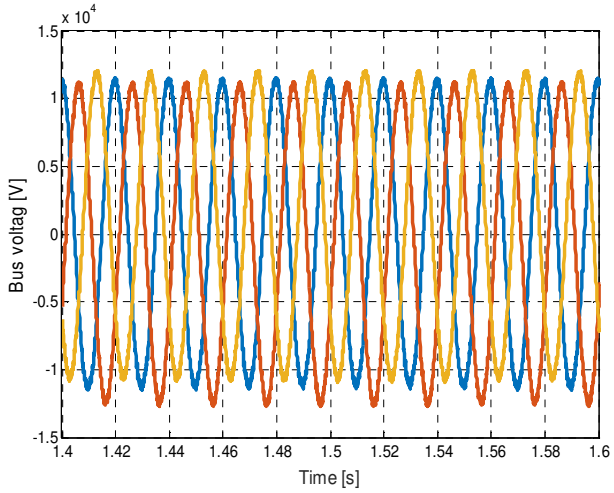

Fig. 12. Bus supply voltages to grid in the charging scenario.

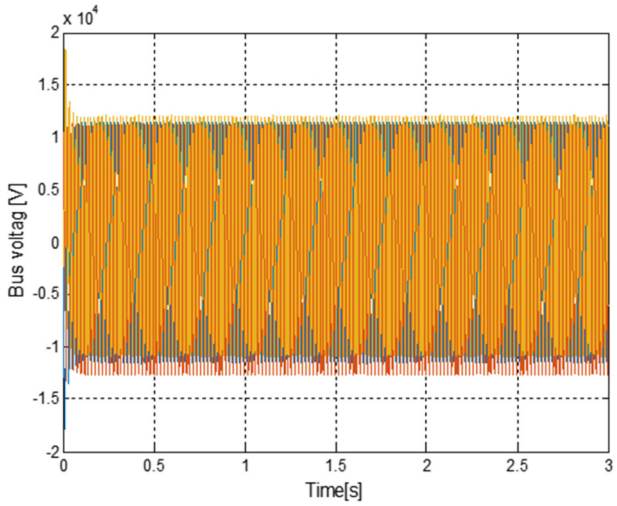

Fig. 13. Bus supply voltages to grid in the discharging scenario.

Fig. 14.

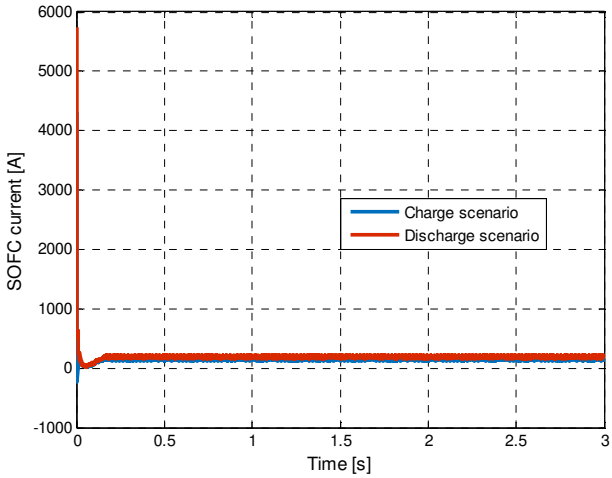

Fig. 15. SOFC currents in the charging and discharging scenarios.

Figure 16 shows the PV currents in the charging and discharging scenarios. In the charging simulation scenario, the PV current decreases from 320 A to 293.8 A for the start-up of the system, and then increases to 296.8 A at 0.208 s, where it is stabilized. The PV current in the discharging simulation scenario takes the same path, but with greater values.

Figure 17 illustrates the supply current of the bus for the charging scenario. The supply current consists of three-level that load power needs. It reaches a lower value at a shorter time, and it is observed that the current exhibits a sinusoidal behavior, indicating that the load is supplied with an alternating current.

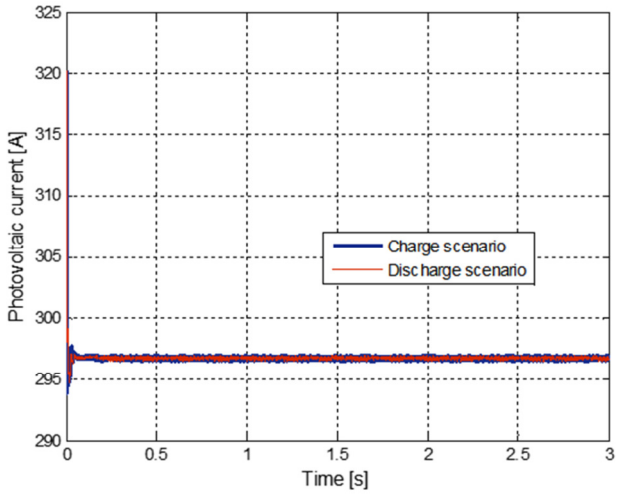

Fig. 16. PV currents in in the charging and discharging scenarios.

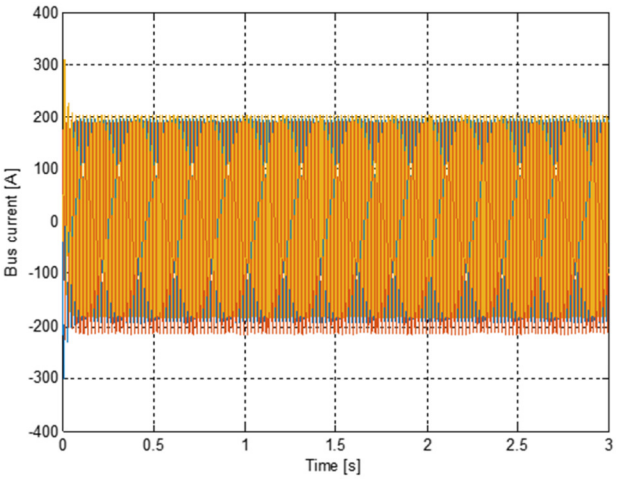

Fig. 17. Supply currents of bus in the charging scenario.

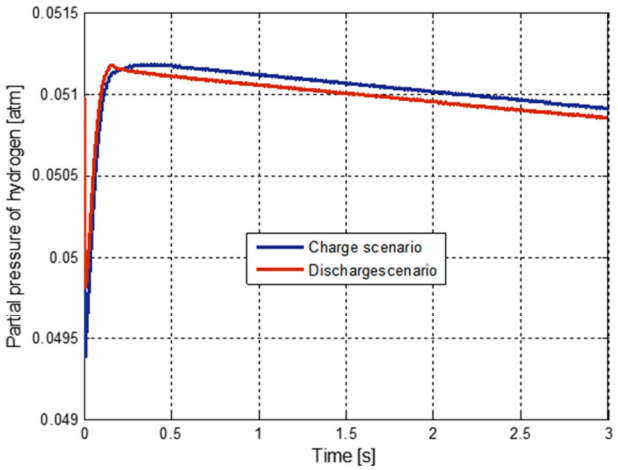

Fig. 18. Partial pressure of hydrogen in the charging and discharging scenarios.

D. The Partial Pressures

Figures 18 and 19 present the partial pressure and the molar flow of hydrogen in the charging and discharging scenarios, respectively. The charging scenario begins with a decrease in the partial pressure from 0.0502 atm to 0.0493 atm, then it rises until it reaches 0.0511 atm, and then it decreases again until reaching the value of 0.0509 atm at the end of the simulation. For the discharging scenario, the partial pressure takes the same pattern, but with lower values, because the battery helps the SOFC and the PV systems to ensure the necessary power. The results confirm the exponential aspect of the SOFC mathematical model. The molar flow follows the same exponential path, but in a decreasing form.

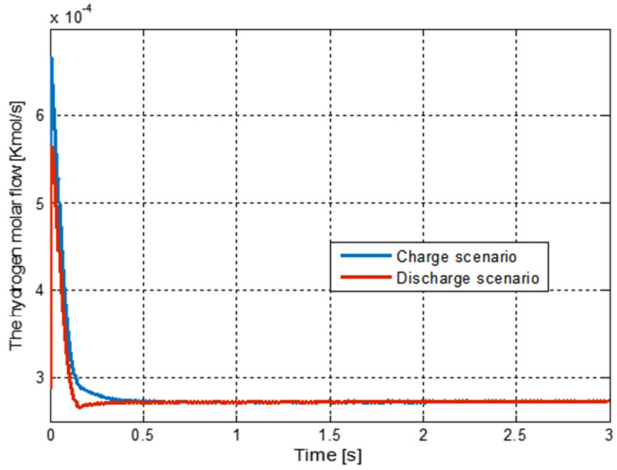

Fig. 19. The molar flow of hydrogen in the charging and discharging scenarios.

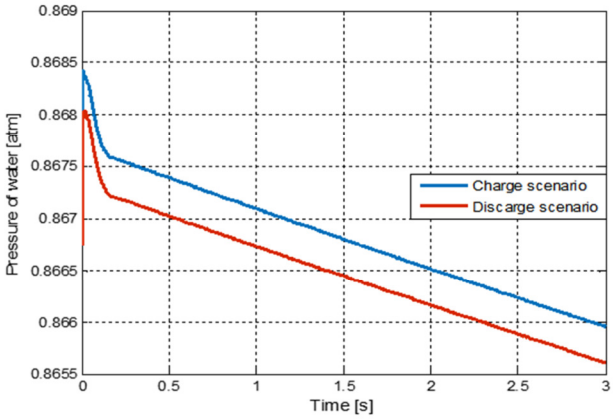

Fig. 20. Partial pressure of water in the charging and discharging scenarios.

Figure 20 shows the partial pressure of the water in the charging and discharging scenarios. It is observed that during charging, the partial pressure starts to increase from 0.867 atm to 0.868 atm and then decreases again until it reaches a final value of 0.866 atm. For the discharging process, the pressure behaves the same way but with lower values, and this is because the battery assists the fuel cell during this stage.

Figure 21 shows the partial pressure of oxygen in the discharging scenario. In the beginning of the discharge, the latter decreases from 0.0509 atm until it reaches a minimum value of 0.0493 atm, then it starts increasing again to reach a maximum value of 0.0520 atm. This corresponds to the start-up of the system. Then the partial pressure of oxygen decreases until it reaches 0.0496 atm at 3 s.

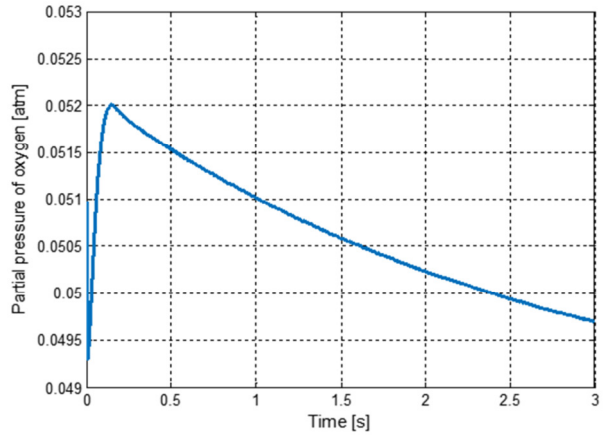

Fig. 21. Partial pressure of oxygen in the discharging scenario.

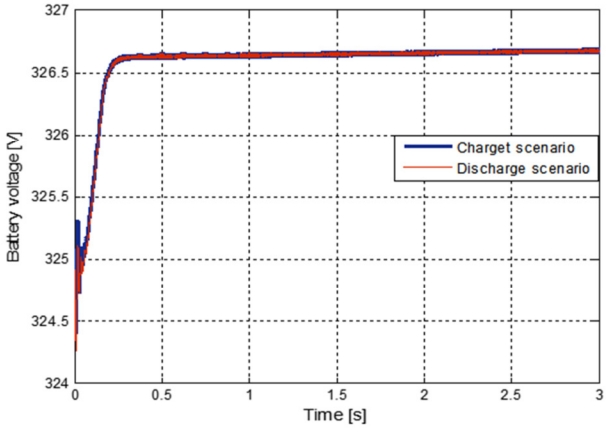

Fig. 22. Battery voltage during the charging and discharging scenarios.

E. Battery Parameters

Figure 22 displays the battery voltage for both the charge charging and discharging scenarios. The charging scenario begins with an increase in the voltage from 324.4 V to 325.3 V, which is the start-up of the system. Then it decreases until it reaches 324.7 V, and then rises again until it reaches 326.6 V and stabilizes. For the discharging scenario, the battery voltage follows the same pattern, but with lower values. The results confirm the exponential aspect of the battery mathematical model.

Figures 23 and 24 show the battery current during the charging and discharging scenarios, respectively. During charging, the battery current decreases from -0.001 A to -52.69 A, and then increases until it reaches 100.7 A at 0.204 s (system start up). It is maintained at this value until the end of the charge. In the discharging scenario, the battery current rises from -0.001 A to 26.68 A, then decreases until it reaches -99.96 A at 0.241 s, and is maintained at this value until the end of the simulation.

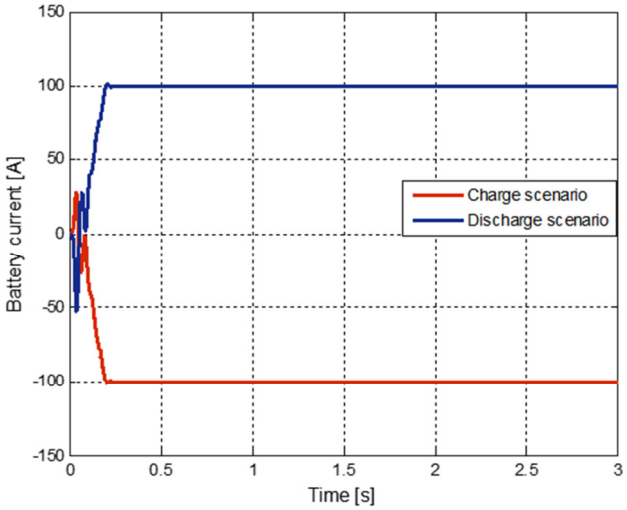

Fig. 23. Battery current during the charging and discharging scenarios.

Figures 24 and 25 present the battery state of charge in the charging and discharging scenarios, respectively. During the charging period, the battery state of charge increases from 70% to 70.012%; and during the discharging period, it inversely decreases from -70% to -70.012%.

Figure 25 depicts the impact of the battery's current density variations on the changes in its voltage over time. The battery current follows the same path: it decreases from 349.3 A until it reaches the 275.1 A. However, it takes different periods, as the voltage becomes greater, the current takes a shorter time to reach the value of 257.1 A (32.5 A at 21.46 h, 13 A at 53.66 h, 6.5 A at 107.3 h).

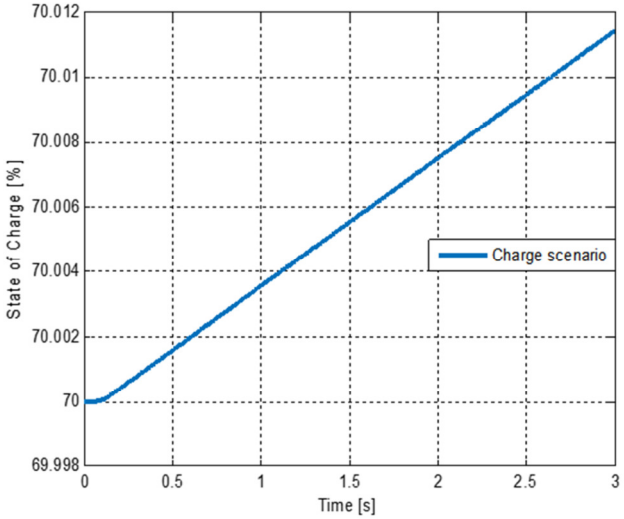

Fig. 24. Battery state of charge during the charging scenario.

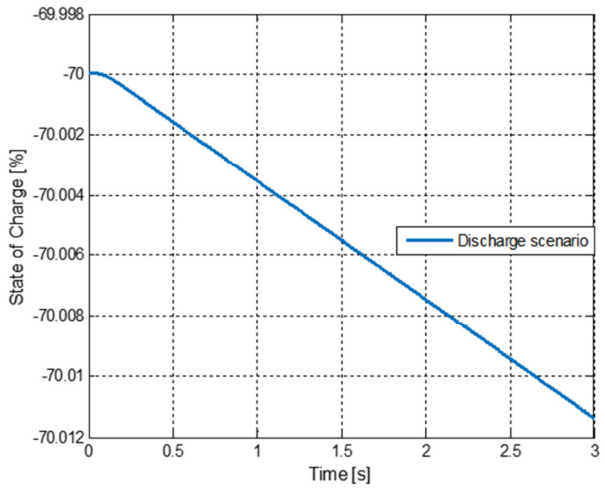

Fig. 25. Battery state of charge during the discharging scenario.

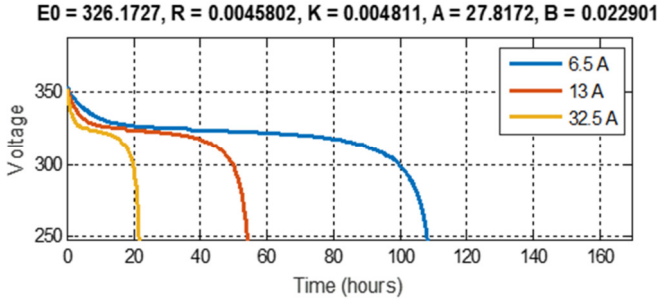

Fig. 26. Impact of the battery's current density variations on the changes in its voltage over time.

VI. CONCLUSION

This paper presents a hybrid renewable energy system management approach using an artificial intelligence-based Multi-Input Multi-Output Fuzzy Logic Control (MIMO-FLC) combined with storage batteries. The simulation results demonstrate that the fuzzy logic–based power management effectively controls the power flow, ensuring a continuous, efficient, and reliable supply to the load under varying conditions. Moreover, the controller provides stability to the overall system operation.

The hybrid Solid Oxide Fuel Cell (SOFC)/ Photovoltaic (PV) system accurately and rapidly tracks the power demand without steady-state oscillations. The MIMO-FLC smooths the battery current, which enhances the battery lifespan and reduces the settling time. This model shows promise for applications in various fields, such as rural electrification.

The simulations also offer insights into the impact of the charging and discharging processes on the hybrid system consisting of an SOFC, a PV array, and a storage battery. The results validate the system's capability to meet the 1 MW load demand reliably.

REFERENCES

[1] I. Laib, A. Hamidat, M. Haddadi, N. Ramzan, and A. G. Olabi, "Study and simulation of the energy performances of a grid-connected PV system supplying a residential house in north of Algeria," *Energy*, vol. 152, pp. 445–454, Jun. 2018, https://doi.org/10.1016/j.energy.2018.03.157.

[2] A. Alazazmeh, A. Ahmed, M. Siddiqui, and M. Asif, "Corrigendum to 'Real-time data-based performance analysis of a large-scale building applied PV system' [Energy Rep. 8 (2022) 15408–15420]," *Energy Reports*, vol. 10, Nov. 2023, Art. no. 2899, https://doi.org/10.1016/j.egyr.2023.09.083.

[3] I. Bendaas, K. Bouchouicha, S. Semaoui, A. Razagui, S. Bouchakour, and S. Boulahchiche, "Performance evaluation of large-scale photovoltaic power plant in Saharan climate of Algeria based on real data," *Energy for Sustainable Development*, vol. 76, Oct. 2023, Art. no. 101293, https://doi.org/10.1016/j.esd.2023.101293.

[4] M. M. Samy, S. Barakat, and H. S. Ramadan, "A flower pollination optimization algorithm for an off-grid PV-Fuel cell hybrid renewable system," *International Journal of Hydrogen Energy*, vol. 44, no. 4, pp. 2141–2152, Jan. 2019, https://doi.org/10.1016/j.ijhydene.2018.05.127.

[5] H. Wang, Z. Xie, L. Pu, Z. Ren, Y. Zhang, and Z. Tan, "Energy management strategy of hybrid energy storage based on Pareto optimality," *Applied Energy*, vol. 327, Dec. 2022, Art. no. 120095, https://doi.org/10.1016/j.apenergy.2022.120095.

[6] F. Saadaoui, K. Mammar, and M. Habbab, "Energy management of a hybrid energy system (PV / PEMFC and lithium-ion battery) based on hydrogen minimization modeled by macroscopic energy representation," *International Journal of Hydrogen Energy*, vol. 48, no. 53, pp. 20388–20405, Jun. 2023, https://doi.org/10.1016/j.ijhydene.2022.11.140.

[7] J. Luo, S. Gao, X. Wei, and Z. Tian, "Adaptive energy management strategy for high-speed railway hybrid energy storage system based on double-layer fuzzy logic control," *International Journal of Electrical Power & Energy Systems*, vol. 156, Feb. 2024, Art. no. 109739, https://doi.org/10.1016/j.ijepes.2023.109739.

[8] Z. Yang, F. Zhu, and F. Lin, "Deep-Reinforcement-Learning-Based Energy Management Strategy for Supercapacitor Energy Storage Systems in Urban Rail Transit," *IEEE Transactions on Intelligent Transportation Systems*, vol. 22, no. 2, pp. 1150–1160, Feb. 2021, https://doi.org/10.1109/TITS.2019.2963785.

[9] F. Calise, F. L. Cappiello, L. Cimmino, and M. Vicidomini, "Dynamic simulation modelling of reversible solid oxide fuel cells for energy storage purpose," *Energy*, vol. 260, Dec. 2022, Art. no. 124893, https://doi.org/10.1016/j.energy.2022.124893.

[10] A. S. Al-Khayyat, M. J. Hameed, and A. A. Ridha, "Optimized power flow control for PV with hybrid energy storage system HESS in low voltage DC microgrid," *e-Prime - Advances in Electrical Engineering, Electronics and Energy*, vol. 6, Dec. 2023, Art. no. 100388, https://doi.org/10.1016/j.prime.2023.100388.

[11] L. Yin and D. Liu, "Adaptive multistep model predictive control for tubular grid-connected solid oxide fuel cells," *Renewable Energy*, vol. 216, Nov. 2023, Art. no. 119062, https://doi.org/10.1016/j.renene.2023.119062.

[12] J. Zhang *et al.*, "Optimal operation of energy storage system in photovoltaic-storage charging station based on intelligent reinforcement learning," *Energy and Buildings*, vol. 299, Nov. 2023, Art. no. 113570, https://doi.org/10.1016/j.enbuild.2023.113570.

[13] H. Wang, L. Mao, H. Zhang, and Q. Wu, "Multi-prediction of electric load and photovoltaic solar power in grid-connected photovoltaic system using state transition method," *Applied Energy*, vol. 353, Jan. 2024, Art. no. 122138, https://doi.org/10.1016/j.apenergy.2023.122138.

[14] E. O. Prado, P. C. Bolsi, H. C. Sartori, and J. R. Pinheiro, "Design and management of photovoltaic energy in uninterruptible power supplies," *Energy Conversion and Management*, vol. 301, Feb. 2024, Art. no. 118038, https://doi.org/10.1016/j.enconman.2023.118038.

[15] X. Zhang, Y. Zhang, C. Zheng, and F. Chen, "Model construction and performance investigation of compound parabolic concentrator based on satellite solar wing photovoltaic arrays," *Energy*, vol. 285, Dec. 2023, Art. no. 129398, https://doi.org/10.1016/j.energy.2023.129398.

[16] L. Cassayre, B. Guzhov, M. Zielinski, and B. Biscans, "Chemical processes for the recovery of valuable metals from spent nickel metal hydride batteries: A review," *Renewable and Sustainable Energy Reviews*, vol. 170, Dec. 2022, Art. no. 112983, https://doi.org/10.1016/j.rser.2022.112983.

[17] B. Allaoua, K. Asnoune, and B. Mebarki, "Energy management of PEM fuel cell/ supercapacitor hybrid power sources for an electric vehicle," *International Journal of Hydrogen Energy*, vol. 42, no. 33, pp. 21158–21166, Aug. 2017, https://doi.org/10.1016/j.ijhydene.2017.06.209.

[18] M. A. Hartani, M. Hamouda, O. Abdelkhalek, and S. Mekhilef, "Sustainable energy assessment of multi-type energy storage system in direct-current-microgrids adopting Mamdani with Sugeno fuzzy logic-based energy management strategy," *Journal of Energy Storage*, vol. 56, Dec. 2022, Art. no. 106037, https://doi.org/10.1016/j.est.2022.106037.

[19] Z. Kang, Y. Zhao, and D. Kim, "Investigation of enterprise economic management model based on fuzzy logic algorithm," *Heliyon*, vol. 9, no. 8, Aug. 2023, Art. no. e19016, https://doi.org/10.1016/j.heliyon.2023.e19016.

[20] M. Ali, Y. Haitao, Z. Che, and Z. Din, "Control of Free Piston Stirling Linear Generator system connected with dc/dc converter for energy storage applications based on SVPWM Rectification Method," *Energy Reports*, vol. 8, pp. 15421–15435, Nov. 2022, https://doi.org/10.1016/j.egyr.2022.11.095.

[21] J. Ingilala and I. Vairavasundaram, "Investigation of high gain DC/DC converter for solar PV applications," *e-Prime - Advances in Electrical Engineering, Electronics and Energy*, vol. 5, Sep. 2023, Art. no. 100264, https://doi.org/10.1016/j.prime.2023.100264.